The Astrophysical Journal, 956:124 (10pp), 2023 October 20 https://doi.org/10.3847/1538-4357/acf372


# Fast-rotating Blue Straggler Stars in the Globular Cluster NGC 3201*

Alex Billi[1,2], Francesco R. Ferraro[1,2], Alessio Mucciarelli[1,2], Barbara Lanzoni[1,2], Mario Cadelano[1,2], Lorenzo Monaco[3], Mario Mateo[4], John I. Bailey III[5], Megan Reiter[6], and Edward W. Olszewski[7]
[1] Dipartimento di Fisica e Astronomia, Università di Bologna, Via Gobetti 93/2 I-40129 Bologna, Italy; alex.billi2@unibo.it
[2] INAF-Osservatorio di Astrofisica e Scienze dello Spazio di Bologna, Via Gobetti 93/3 I-40129 Bologna, Italy
[3] Instituto de Astrofísica, Facultad de Ciencias Exactas, Universidad Andres Bello, Sede Concepcion, Talcahuano, Chile
[4] Department of Astronomy, University of Michigan, 1085 S. University, Ann Arbor, MI 48109, USA
[5] Department of Physics, UCSB, Santa Barbara, CA 93016, USA
[6] Department of Physics and Astronomy, Rice University, 6100 Main Street, Houston, 77005-1827, TX, USA
[7] Steward Observatory, The University of Arizona, 933 N. Cherry Avenue, Tucson, AZ 85721, USA
*Received 2023 May 25; revised 2023 August 21; accepted 2023 August 22; published 2023 October 16*

## Abstract

We used high-resolution spectra acquired with the Magellan Telescope to measure radial and rotational velocities of approximately 200 stars in the Galactic globular cluster NGC 3201. The surveyed sample includes blue straggler stars (BSSs) and reference stars in different evolutionary stages (main-sequence turnoff, subgiant, red giant, and asymptotic giant branches). The average radial velocity value ($\langle V_r \rangle = 494.5 \pm 0.5$ km s$^{-1}$) confirms a large systemic velocity for this cluster and was used to distinguish 33 residual field interlopers. The final sample of member stars has 67 BSSs and 114 reference stars. Similarly to what is found in other clusters, the totality of the reference stars has negligible rotation ($< 20$ km s$^{-1}$), while the BSS rotational velocity distribution shows a long tail extending up to $\sim$200 km s$^{-1}$, with 19 BSSs (out of 67) spinning faster than 40 km s$^{-1}$. This sets the percentage of fast-rotating BSSs to $\sim$28%. Such a percentage is roughly comparable to that measured in other loose systems ($\omega$ Centauri, M4, and M55) and significantly larger than that measured in high-density clusters (as 47 Tucanae, NGC 6397, NGC 6752, and M30). This evidence supports a scenario where recent BSS formation (mainly from the evolution of binary systems) is occurring in low-density environments. We also find that the BSS rotational velocity tends to decrease for decreasing luminosity and surface temperature, similarly to what is observed in main-sequence stars. Hence, further investigations are needed to understand the impact of BSS internal structure on the observed rotational velocities.

*Unified Astronomy Thesaurus concepts:* Blue straggler stars (168); Spectroscopy (1558); Globular star clusters (656)

## 1. Introduction

Blue straggler stars (BSSs) are an "exotic" stellar population observed in different stellar environments, such as globular clusters (GCs; Sandage 1953; Ferraro et al. 1997, 1999, 2003, 2006b, 2009; Piotto et al. 2004; Lanzoni et al. 2007; Leigh et al. 2007; Dalessandro et al. 2008; Moretti et al. 2008), open clusters (Carraro et al. 2008; Mathieu & Geller 2009; Geller & Mathieu 2011; Gosnell et al. 2014), dwarf spheroidal galaxies (Momany et al. 2007; Mapelli et al. 2009), and the Milky Way halo and bulge (Preston & Sneden 2000; Clarkson et al. 2011). In the color–magnitude diagram (CMD), BSSs lie on a bluer extension of the main sequence (MS) and have luminosities brighter than the MS turnoff. Hence, BSSs are more massive than MS stars ($M \sim 1.2$–$1.6\ M_{\odot}$; Shara et al. 1997; Gilliland et al. 1998; De Marco et al. 2005; Fiorentino et al. 2014; Raso et al. 2019). Because of their relatively large mass, BSSs are crucial "gravitational test particles" to probe the internal dynamics of GCs (e.g., Ferraro et al. 2009, 2012, 2020). In this respect, Ferraro et al. (2012) introduced the concept of a "dynamical clock," an empirical method to measure the level of dynamical evolution of star clusters by using the BSS radial distribution. This concept was further refined by the definition of the $A^{+}_{\rm rh}$ parameter (Alessandrini et al. 2016; Lanzoni et al. 2016), which quantifies the level of BSS central segregation with respect to a lighter (reference) population and has been successfully adopted to rank a large sample of Galactic (Ferraro et al. 2018a, 2023) and extra-Galactic star clusters (Ferraro et al. 2019; Dresbach et al. 2022) in terms of their dynamical stage.

The formation and evolutionary processes of BSSs are still not completely understood although much progress in the observational characterization and theoretical modeling of these stars has been made in recent years, especially in open clusters (see, e.g., Mathieu & Geller 2009; Perets & Fabrycky 2009; Chatterjee et al. 2013; Leiner & Geller 2021; Jiang 2022; Reinoso et al. 2022; Cordoni et al. 2023 and references therein). Three main formation scenarios have been suggested so far: (i) mass-transfer activity in binary systems (McCrea 1964), where a companion star transfers mass and angular momentum to the accreting proto-BSS, (ii) direct collisions between two or more stars (Hills & Day 1976), and (iii) mergers/collisions induced by dynamical/stellar evolution in triple systems (see Andronov et al. 2006; Perets & Fabrycky 2009). The latter is thought to play a major role in the field and in open clusters, and it naturally accounts for the observed period-eccentricity distribution of BSS binaries (Perets & Fabrycky 2009). The mass-transfer scenario is expected to be dominant in low-density systems (see, e.g., Mateo et al. 1990;

* Based on observations collected at the Clay Magellan Telescope, located at Las Campanas Observatory (Chile).

Sollima et al. 2008; Mathieu & Geller 2009), and photometric confirmation of this formation channel has been recently obtained in open clusters through the detection of ultraviolet emission from hot white dwarf companions (the peeled donor stars) to a few BSSs (Gosnell et al. 2014, 2015). A potential spectroscopic signature of BSS formation through mass-transfer activity has been also identified in a few BSSs in Galactic GCs. In fact, at odds with collisional BSSs (Lombardi et al. 1995), mass-transfer BSSs are predicted to show carbon and oxygen depletion on their surface (Sarna & De Greve 1996) due to the accretion of material coming from the innermost layers of the donor star, which are expected to be partially processed by the CNO burning cycle. Ferraro et al. (2006a) and Lovisi et al. (2013a) detected carbon and oxygen depletion in a subsample of BSSs in 47 Tucanae and M30, respectively. On the other side, subpopulations of collisional BSSs have been possibly identified in the CMD of a few post-core-collapsed GCs (Ferraro et al. 2009; Portegies Zwart 2019; Dalessandro et al. 2013; Beccari et al. 2019; Cadelano et al. 2022), where they appear all aligned along a narrow blue sequence, well separated from the remaining population of redder BSSs. The formation of these collisional BSSs is thought to be promoted by the enhanced collisional activity occurring in the cluster core during the core collapse and the post-core-collapse stages, when the central density substantially increases.

The study of rotational velocities can add an important piece to the BSS formation puzzle, providing additional constraints to their origin and evolutionary processes. From a theoretical point of view, large rotational velocities are expected at birth for both mass-transfer BSSs (Sarna & De Greve 1996) and collisional BSSs (Benz & Hills 1987), but some braking mechanisms (such as magnetic braking and disk locking) should then intervene to slow down these stars with efficiencies and timescales that are not fully understood yet (e.g., Leonard & Livio 1995; Sills et al. 2005). Recent results in open clusters suggest that magnetic braking is efficient enough to slow down mass-transfer BSSs in timescales shorter than 1 Gyr (Leiner et al. 2018). In fact, the relation between the measured BSS rotation periods and ages (derived from the cooling time of the white dwarf companion) is well reproduced by the same models used to describe the spin-down rate of single, low-mass MS stars (which, indeed, share the same structure in terms of convective envelopes and magnetic fields; Gallet & Bouvier 2015). This result indicates that the BSS rotation rate can potentially be used as a gyro-chronometer to measure the time since the end of mass transfer. Additional complexity is introduced by phenomena like the synchronization of close binaries (e.g., Hut 1981), which tends to spin up the stars but is very hard to constrain observationally since it requires dedicated multi-epoch observations in both photometry and spectroscopy (see, e.g., Meibom et al. 2006; Lurie et al. 2017; Leiner et al. 2019 and references therein).

In this context, several years ago, our group started an extensive high-resolution spectroscopic survey with large ground-based telescopes for eight Galactic GCs with different structural parameters, with the aim to provide the rotational velocities of a representative sample of BSSs formed and evolved in different environments. The results obtained for six clusters have been already published: see Ferraro et al. (2006a) for 47 Tucanae; Lovisi et al. (2010, 2012, 2013a, 2013b) for M4, NGC 6397, M30, and NGC 6752, respectively; and Mucciarelli et al. (2014) for $\omega$ Centauri. These data, complemented with the results obtained for NGC 3201 (which are presented in this paper) and for M55 (which will be discussed in A. Billi et al. 2023, in preparation) have been recently used by Ferraro et al. (2023) to demonstrate that the fraction of fast-rotating BSSs (with $v \sin(i) \geqslant 40$ km s$^{-1}$, with $i$ being the inclination angle on the plane of the sky) anticorrelates with the central density of the host system, decreasing from $\sim$40% to $\sim$5% when the central density increases from $\log \rho_0 = 2.5$ to $\log \rho_0 = 5$ (in units of solar luminosity per cubic parsec), thus indicating the tendency of fast-spinning BSSs to populate low-density environments.

The present paper is devoted to discussing the results obtained for 67 BSSs observed in NGC 3201 at a spectral resolution $R = 18{,}000$ and compare them to the rotational velocities measured by Simunovic & Puzia (2014, hereafter, SP14) for 37 such objects in the same cluster, at $R = 10{,}000$. The paper is organized as follows: the observations are presented in Section 2, and the determinations of radial velocities, atmospheric parameters, and rotational velocities are discussed in Sections 3, 4, and 5, respectively. Section 6 discusses the comparison between our findings and those of SP14. A summary of the results and the conclusions of the work are provided in Section 7.

## 2. Observations

This work is based on stellar spectra acquired with the multi-object spectrograph Michigan/Magellan Fiber System (M2FS; Mateo et al. 2012) mounted on the Clay Magellan Telescope, located at Las Campanas Observatory (Chile). M2FS is composed of two spectrographs fed by 128 fibers each. The observations have been performed during two nights (on 2019 February 28 and March 2), adopting the $\mathrm{Mgb}_{\mathrm{Revb}}$ configuration, which covers the spectral region between 5127 and 5184 Å, sampling the first two lines of the Mg triplet (at 5167.3 and 5172.6 Å) with a spectral resolution $R \sim 18{,}000$. Two different fiber configurations have been adopted to secure spectra for approximately 200 targets in the cluster direction. A total of six exposures of 30 minutes each and 10 exposures of 20 minutes have been secured on the first and second night, respectively.

The BSS selection has been performed on the basis of high-resolution ultraviolet catalogs obtained from Hubble Space Telescope observations for the central regions of NGC 3201 and optical ground-based observations for the external regions (see Ferraro et al. 2023). For a proper comparison with SP14, particular care has been devoted to include in the sample most of the BSSs observed in that work (29 out 37). In addition, to compare the BSS rotational velocities with those of "normal" cluster stars, we simultaneously observed a significant sample of reference objects distributed in different evolutionary stages. Due to the high value of the seeing (larger than 1.″50), two and three exposures from the first and the second night, respectively, have been excluded from the analysis. As a result, we secured spectra of 67 BSSs, 9 subgiant branch (SGB) stars, 1 MS star, 98 red giant branch (RGB) stars, and 6 asymptotic giant branch (AGB) stars. Figure 1 shows the position of the observed sample in the proper-motion-selected and differential-reddening-corrected CMD of NGC 3201, obtained from the photometric catalog of the Stetson database (Stetson et al. 2019) by applying the

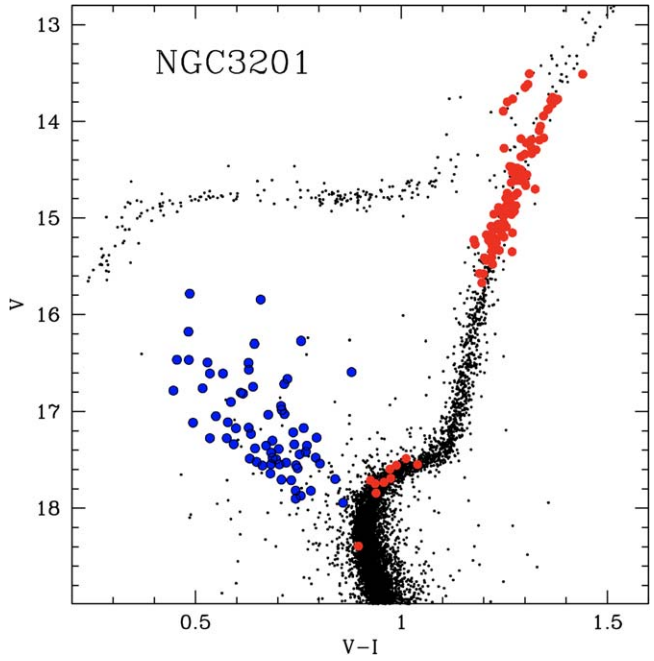


**Figure 1.** Proper-motion-selected and differential-reddening-corrected CMD of NGC 3201 (black dots), with the spectroscopic targets discussed in the paper highlighted as solid colored circles: the 67 BSSs are marked in blue, while the reference sample of MS, SGB, RGB, and AGB stars are plotted in red.

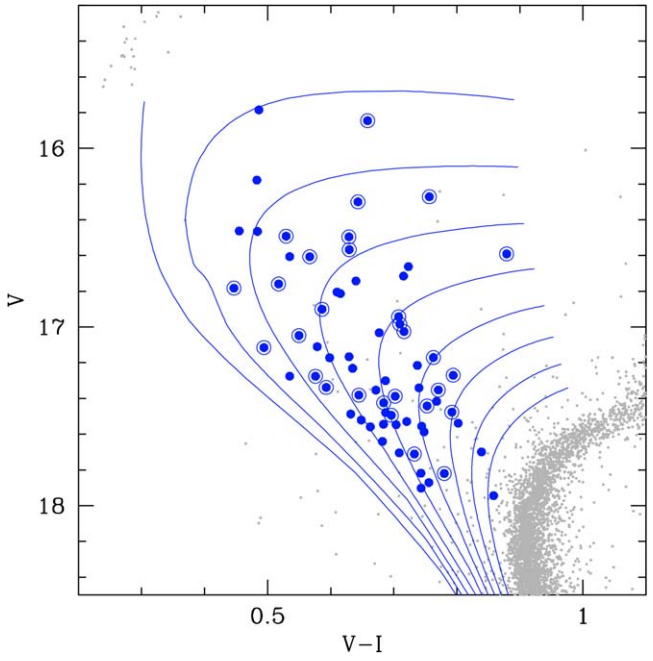


**Figure 3.** CMD of NGC 3201 (gray dots) with the 67 surveyed BSSs marked as blue circles, and a set of BaSTI isochrones (Pietrinferni et al. 2021) with ages ranging from 1 to 9 Gyr overplotted as blue lines. The BSSs in common with SP14 are encircled.

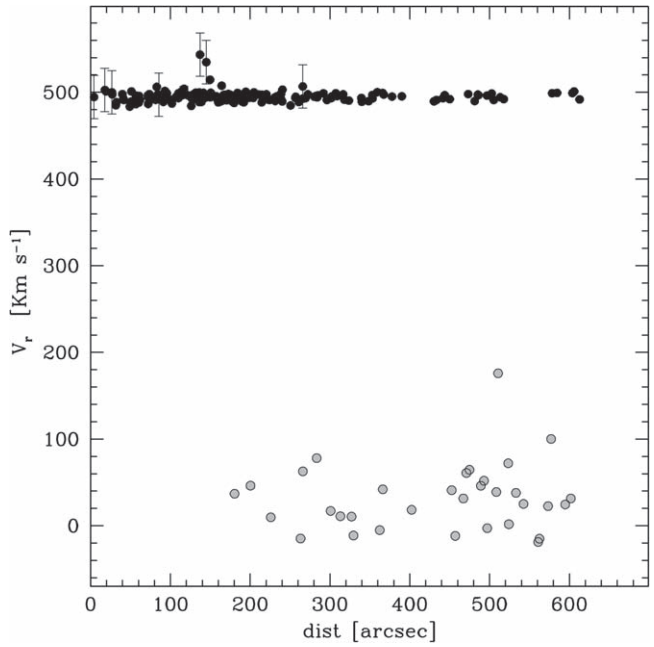


**Figure 2.** Radial velocities (in kilometers per second) of the target stars as a function of their distance from the cluster center (in arcseconds). The stars belonging to NGC 3201 are shown as black circles, while the objects belonging to the Galactic field are colored in gray.

method described in Cadelano et al. (2020; see also Deras et al. 2023).

## 3. Radial Velocities and Cluster Membership

The raw spectra have been pre-reduced by following the standard procedure including bias subtraction, flat-field correction, wavelength calibration, and, finally, the 1D spectra extraction. The median of the sky spectra secured during the observations has been assumed as the master-sky spectrum and used to remove the sky contribution from each individual exposure. Then, for each target the sky-subtracted spectra have been combined, providing the final spectrum for the analysis. The radial velocities of the sampled stars have been measured by using the IRAF task fxcor, which performs a cross correlation between the observed spectrum and a template of known radial velocity (Tonry & Davis 1979). As templates we adopted synthetic spectra computed with the code SYNTHE (Sbordone et al. 2004; Kurucz 2005) by adopting the last version of the Kurucz/Castelli line list for atomic and molecular transitions. To take into account the different stellar parameters and line strengths, we defined a template for giant (RGB and AGB) stars and another one for BSSs and SGB/turnoff stars. The model atmospheres have been computed with the ATLAS9 code (Kurucz 1993; Sbordone et al. 2004) under the assumptions of local thermodynamic equilibrium and plane-parallel geometry and by adopting the new opacity distribution functions by Castelli & Kurucz (2003) with no inclusion of overshooting (Castelli et al. 1997).

Figure 2 shows the distribution of the measured radial velocities as a function of the distance from the cluster center. Here we adopt the center of gravity obtained by B. Lanzoni et al. (2023, in preparation): $\alpha_{J2000} = 10^h17^m36^s.82$, $\delta_{J2000} = -46°24'44''.9$. The acquired data set extends from $r = 4''$ out to $\sim 630''$. The cluster population (black circles) is clearly distinguishable as a narrow component strongly peaked at the large systemic velocity of the cluster: $V_{sys} = 494.5 \pm 0.5$ km s$^{-1}$ (Ferraro et al. 2018b). This allows a straightforward identification of the few field stars included in the observed sample, which show much smaller radial velocities (gray circles in Figure 2). The few cluster members showing radial velocities larger than the average are rapidly rotating BSSs for which the measures are more uncertain because of the significant deformation of the absorption lines (see Section 5).

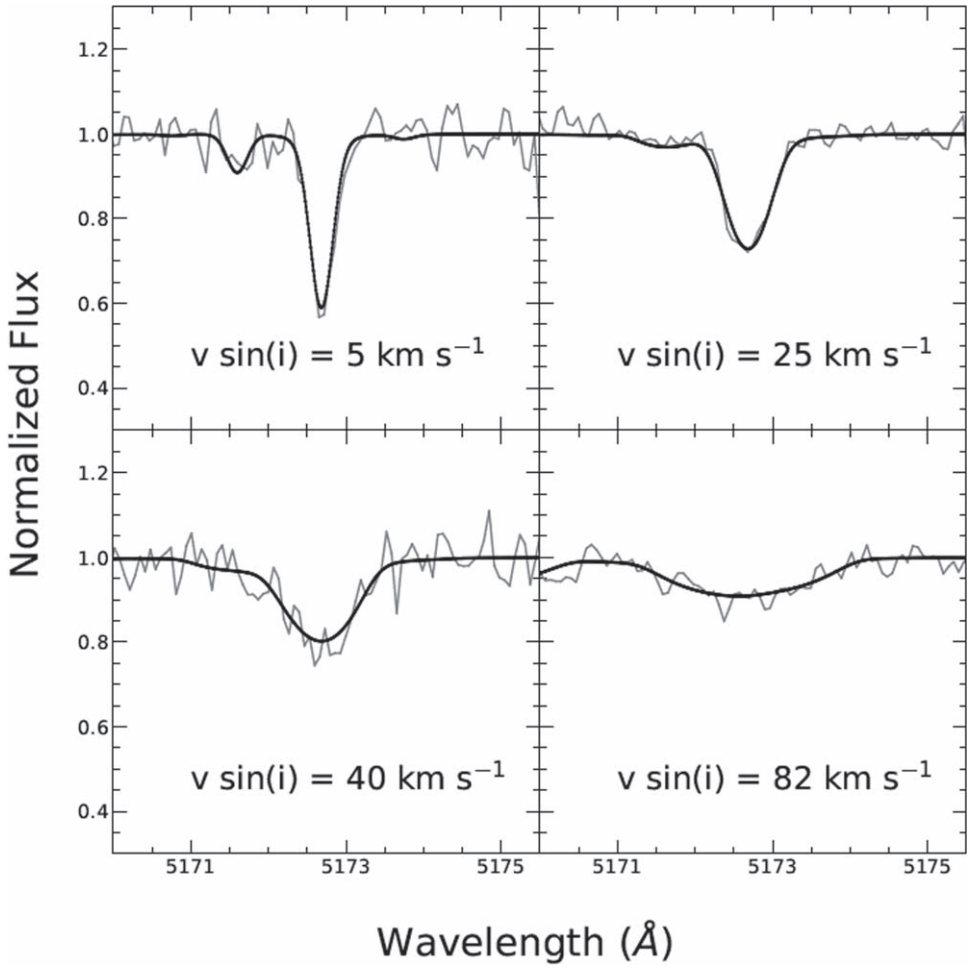


**Figure 4.** Comparison between the observed spectra (gray lines) and the best-fit synthetic spectra (black lines) for four BSSs with different rotational velocities, ranging from 5 to 82 km s$^{-1}$.

## 4. Atmospheric Parameters

To estimate the effective temperature ($T_{\rm eff}$) and the surface gravity ($\log g$) of the observed BSSs, we have compared their CMD location with a set of $\alpha$-enhanced BaSTI isochrones (Pietrinferni et al. 2021), computed by assuming the cluster metallicity ([Fe/H] = −1.55), and ages ranging between 1 and 9 Gyr. The models have been reported to the observed CMD (see blue lines in Figure 3) by adopting an apparent distance modulus $(m-M)_V = 14.20$ and a color excess $E(B-V) = 0.27$, in agreement with Harris (1996). As is apparent from the figure, the grid of isochrones properly samples the portion of the CMD where BSSs are distributed. Hence, the needed values of $T_{\rm eff}$ and $\log g$ have been determined by projecting each BSS onto the closest isochrone. The resulting effective temperatures vary between 6700 and 8700 K, while $\log g$ ranges between 3.6 and 4.3 dex. An analogous procedure, but using the 12 Gyr old isochrone, has been performed for the reference stars. It is worth emphasizing that these photometric estimates of temperature and gravity are accurate enough to guarantee a solid determination of the rotational velocity. In fact, the impact of these two parameters on the measured rotation is modest. For instance, even large variations in temperature and gravity (±300–500 K in $T_{\rm eff}$ and ± 0.8 dex in $\log g$) produce a small effect (∼1 km s$^{-1}$) in the measured value of $v\sin(i)$. In addition, we assumed a microturbulence velocity of 1 km s$^{-1}$ for the BSSs and 1.5 km s$^{-1}$ for the giant stars although different assumptions for this parameter have no impact on the rotational velocity values.

## 5. Rotational Velocities

The rotational velocities (projected on the plane of the sky) have been calculated by using a $\chi^2$ minimization procedure between the observed spectra and a grid of synthetic spectra calculated for the atmospheric parameters estimated as described in Section 4 and for different values of $v\sin(i)$. The rotational velocity has been measured from the two first lines of the Mg triplet at 5167.3 and 5172.6 Å. These two features are strong enough to allow an accurate measure of $v\sin(i)$ also in the case of very large rotations (of the order of 100 km s$^{-1}$). For the sake of illustration, Figure 4 shows the comparison between the observed and the synthetic spectra of four stars with different rotational velocities for the line at 5172.6 Å. As can be seen, the absorption line is still clearly visible also in the star rotating at more than 80 km s$^{-1}$.

The uncertainties in the measured rotational velocities have been determined through Monte Carlo simulations. For each star we calculated a synthetic spectrum adopting the atmospheric parameters and rotational velocity previously obtained. Then, through the random additions of Poissonian noise, we simulated 300 spectra with the same signal-to-noise ratio of the observed one. These have been analyzed as described above in Section 3, each time obtaining the best-fit rotational velocity

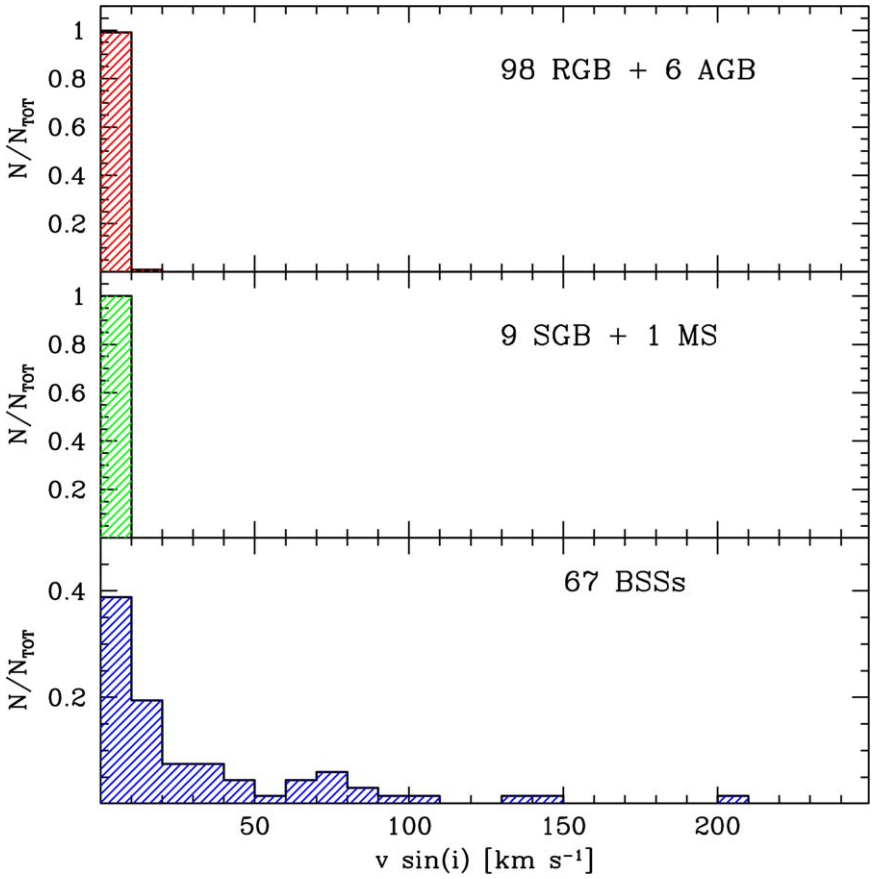


**Figure 5.** Distributions of the rotational velocities measured for highly evolved, giant stars (red histogram in the upper panel), mildly evolved (SGB and MS) stars (green histogram in the central panel), and BSSs (blue histogram in the bottom panel).

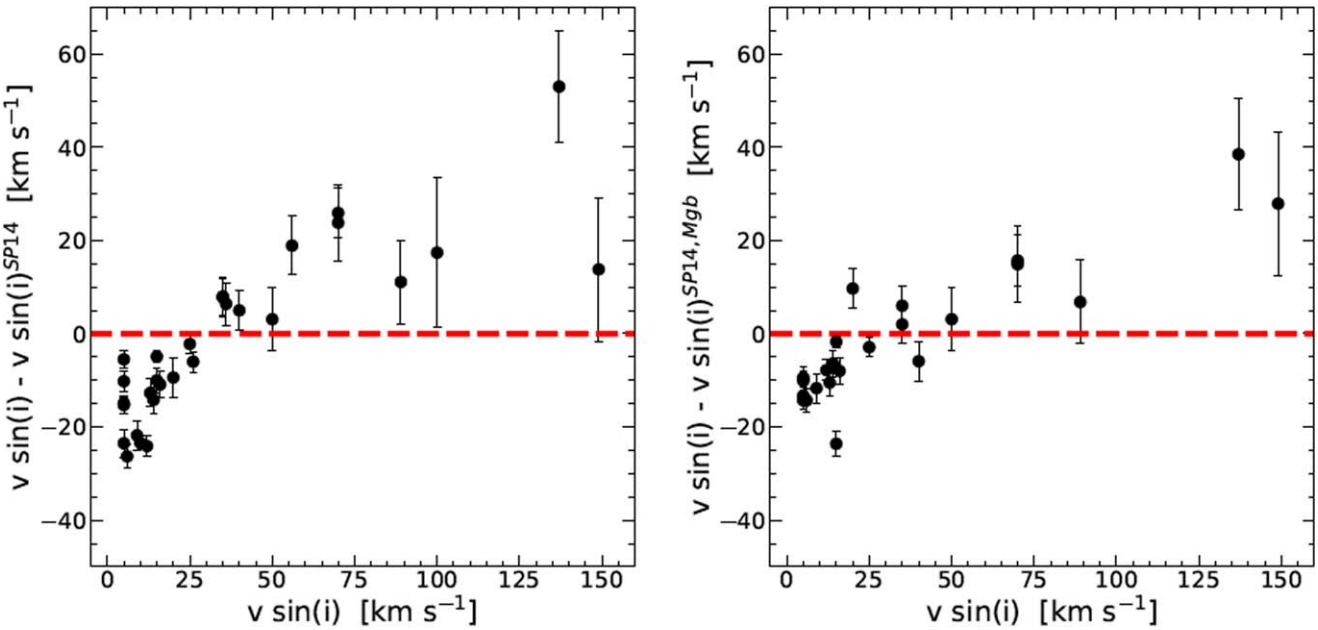


**Figure 6.** Left panel: difference between the rotational velocities obtained in this work ($v \sin(i)$) and those determined by SP14 ($v \sin(i)^{SP14}$) for the 29 BSSs in common, as a function of our measures. Right panel: as in the left panel but for the rotational velocities of SP14 computed from the Mgb triplet line alone ($v \sin(i)^{SP14,\ Mgb}$).

value. The standard deviation of the derived velocity distribution has been assumed as $1\sigma$ uncertainty in the rotational velocity of each star. The estimated uncertainties range from a few (2–5) km s$^{-1}$ for slowly rotating stars, up to 15–20 km s$^{-1}$ for the fast-spinning targets (with rotation of the order of, or larger than, 100 km s$^{-1}$).

As shown in Figure 5, the distributions of rotational velocities obtained for the observed samples of BSSs and

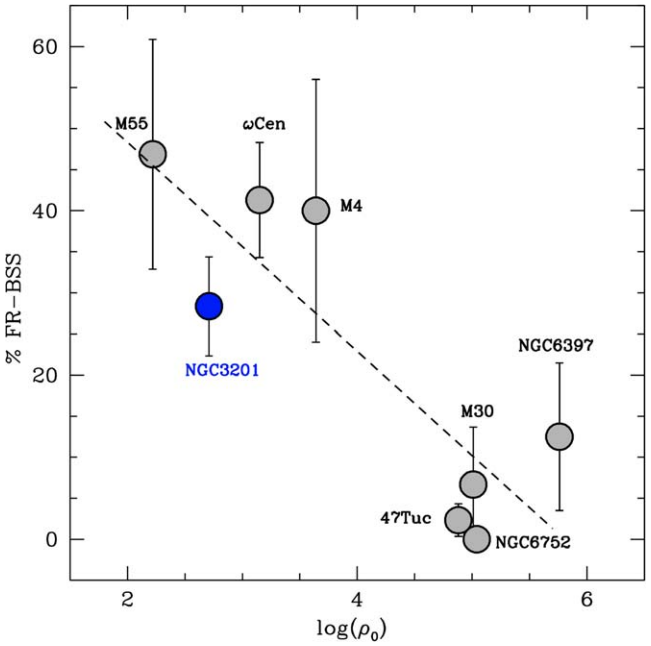


**Figure 7.** Percentage of FRs (i.e., number of BSSs with $v \sin(i) > 40$ km s$^{-1}$ over the total number of surveyed BSSs) as a function of the central density of the parent cluster for NGC 3201 (blue circle) and the other GCs (namely, M55, $\omega$ Centauri, M4, 47 Tucanae, M30, NGC 6752, and NGC 6397; gray circles) studied in Ferraro et al. (2023).

normal cluster stars are strikingly different. Almost all the highly evolved stars (RGB and AGB targets), all the SGB stars, and the MS star in the sample show negligible rotation ($v \sin(i) < 10$ km s$^{-1}$), in agreement with the rotational velocities quoted in the literature for cluster and field stars in similar evolutionary stages (see, e.g., Lucatello & Gratton 2003; Cortés et al. 2009; De Medeiros et al. 2014). Indeed, only one RGB star has a rotation of 12 km s$^{-1}$, which could be due to an interaction with a companion object (unfortunately our data set is not suitable to search for radial velocity variability, but this object is certainly worthy of further investigations). Conversely, the distribution of BSS rotational velocities appears to be much more articulated, with a peak at low values followed by a long tail extending up to very large rotations (up to 207 km s$^{-1}$). Moreover, only less than 40% of the entire sample shows rotational velocities below 10 km s$^{-1}$, while 19 BSSs of our 67 (∼28% of the total) spin faster than 40 km s$^{-1}$ and, according to the definition of Ferraro et al. (2023), are classified as fast rotators (FRs). Hence, this comparison clearly demonstrates that BSSs display a very peculiar rotational velocity distribution with respect to normal cluster stars.

## 6. Comparison with SP14

As mentioned in Section 1, SP14 determined the rotational velocities of 37 BSSs in NGC 3201 (plus other BSSs in $\omega$ Centauri and NGC 6218) from the analysis of spectra acquired with the Inamori Magellan Areal Camera and Spectrograph on the Baade Magellan Telescope, at a spectral resolution $R = 10{,}000$. The rotational velocity distribution derived by the authors of SP14 is different from that plotted in Figure 5: it shows a peak at 25–30 km s$^{-1}$, which is not visible in our distribution, and only six stars (∼19% of the total sample) spin faster than 40 km s$^{-1}$. Since we have 29 BSSs in common with SP14, we can perform a proper star-to-star comparison to understand the origin of the discrepancy.

Figure 6 shows the difference between the rotational velocities determined in this work and in SP14 as a function of our measures for the 29 BSSs in common. As is apparent, all the stars for which we find $v \sin(i) < 30$ km s$^{-1}$ have larger rotation in SP14 (in some extreme cases, they are in excess by even ∼25 km s$^{-1}$), while the opposite is true for most of the FRs. This trend is very similar to that found by Mucciarelli et al. (2014) in the case of $\omega$ Centauri (see their Figure 6), from the comparison between the measurements of SP14 and those obtained from higher-resolution ($R > 18{,}000$) spectra acquired with FLAMES at the ESO-VLT for 14 BSSs in common. Also taking into account that the spectral resolution used in the present work and in Mucciarelli et al. (2014) is approximately the same and about twice that of SP14, we conclude that the origin of the discrepancies observed in NGC 3201 (Figure 6) and in $\omega$ Centauri (Figure 6 in Mucciarelli et al. 2014) is the same. The disagreement detected at low rotational velocities can be ascribed to the lower spectral resolution used in SP14, which naturally makes much more difficult the measure of small rotation values because the line profile is dominated by the instrumental broadening instead of the rotational broadening.

The difference in the high-velocity regime is mainly ascribable to the different absorption lines used in the SP14 analysis. In fact, in addition to the Mgb triplet, the authors of SP14 also used the Balmer lines and the MgII 4481 line. The Balmer lines, however, are only marginally sensitive to rotation. In fact, as shown in Figure 8 of Mucciarelli et al. (2014), a change of rotational velocity from 0 to 200 km s$^{-1}$ produces no significant variations in the line wing morphology and the full width at half maximum of the Balmer lines. The Mgb triplet lines are by far more sensitive to rotation than the Balmer ones, and the estimates they provide are therefore significantly more precise. This is also confirmed by the fact that the difference between the rotational velocities measured by SP14 from the Mgb triplet alone and the values determined in this work is reduced: the dispersion of the data with respect to zero decreases from $\sigma = 8.7$ to $\sigma = 6.4$ (see Figure 6). Indeed, by using the rotational velocities measured from the Mgb diagnostic alone, the fraction of BSSs spinning faster than 40 km s$^{-1}$ in the SP14 sample amounts to ∼20–25% of the total, which is not that different from what we obtained here (∼28%).

## 7. Discussion and Conclusions

As discussed in Section 1, the BSSs analyzed in this work were part of the sample studied in Ferraro et al. (2023), who found a strong anticorrelation between the fraction of FRs (defined as BSSs spinning at more than 40 km s$^{-1}$)[8] and the central density of the parent cluster, suggesting that loose environments are the ideal habitat for highly rotating BSSs. This is shown in Figure 7, which is a reproduction of Figure 3 of Ferraro et al. (2023) and where the position of NGC 3201 is highlighted in blue. As can be seen, the percentage of FRs in NGC 3201 is fully compatible with that of the other low-density clusters in the sample (namely, M55, $\omega$ Centauri, and

[8] The 40 km s$^{-1}$ threshold was adopted from the inspection of the BSS rotational velocity distributions in eight GCs. Ferraro et al. (2023) also showed that by adopting a slightly different threshold (30 or 50 km s$^{-1}$), the overall results remain unchanged.

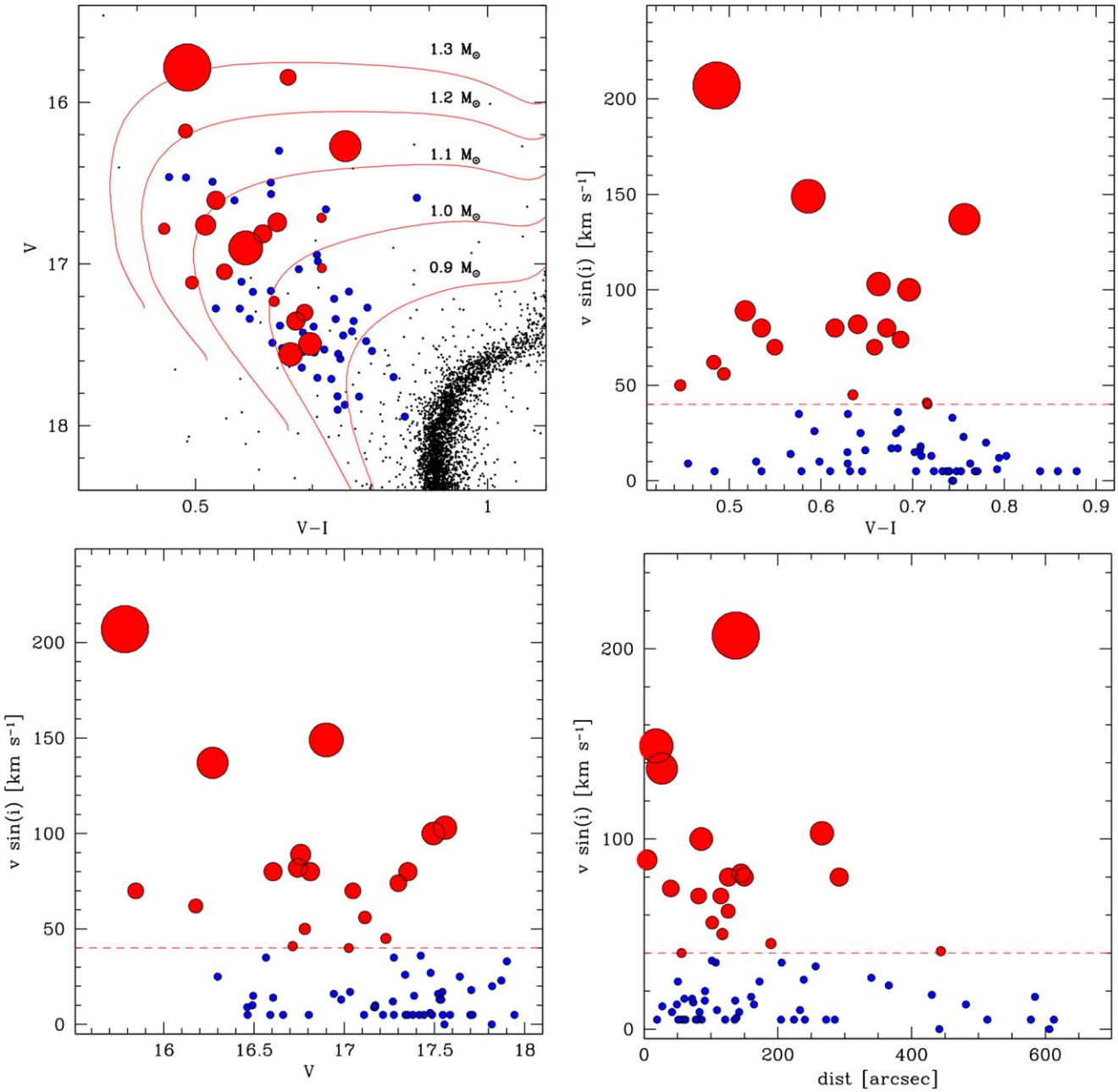


**Figure 8.** From top left to bottom right: distribution of the surveyed BSSs in the CMD of NGC 3201, rotational velocity distributions as a function of the $(V - I)$ color, the $V$ magnitude, and the distance from the cluster center. In all the panels, the FRs are plotted as red circles with increasing size for increasing rotational velocity, while the BSSs spinning at $v \sin(i) < 40$ km s$^{-1}$ are marked as small blue circles. A set of single-mass evolutionary tracks (Pietrinferni et al. 2021) for stars between 0.9 and 1.3 $M_{\odot}$ are also overplotted as red solid lines in the top left panel.

M4), while it is significantly larger than that measured in the four high-density systems (namely, 47 Tucanae, M30, NGC 6752, and NGC 6397).

High-rotational velocities are expected to be a characteristic feature of recently born BSSs in both the proposed formation scenarios as the natural effect of angular momentum accretion during mass transfer (Packet 1981; de Mink et al. 2013) and angular momentum conservation during the contraction phase in the post-collision evolution (e.g., Benz & Hills 1987; Sarna & De Greve 1996). Then, a progressive slowdown of these stars due to the occurrence of some braking mechanisms (like magnetic braking or disk locking) is predicted, but the efficiencies of these processes are still unknown (Leonard & Livio 1995; Sills et al. 2005). A few constraints are finally emerging from the analysis of BSSs in open clusters (Leiner et al. 2018) and in post-core-collapse systems (Ferraro et al. 2023), both indicating a braking timescale of the order of 1–2 Gyr for both mass-transfer and collisional BSSs. Following this scenario, a large rotational velocity can be considered as the signature of the early phase of BSS evolution, and the percentage of FRs therefore provides information about the recent BSS formation activity in the host cluster. On the other hand, stellar collisions are expected to be negligible in low-density environments, where the main BSS formation channel likely is mass transfer in binary systems. Indeed, the fraction of FRs has been found to also correlate with the fraction of binaries (see Figure 4 of Ferraro et al. 2023). Hence, the significantly larger fraction of FRs measured in loose than in

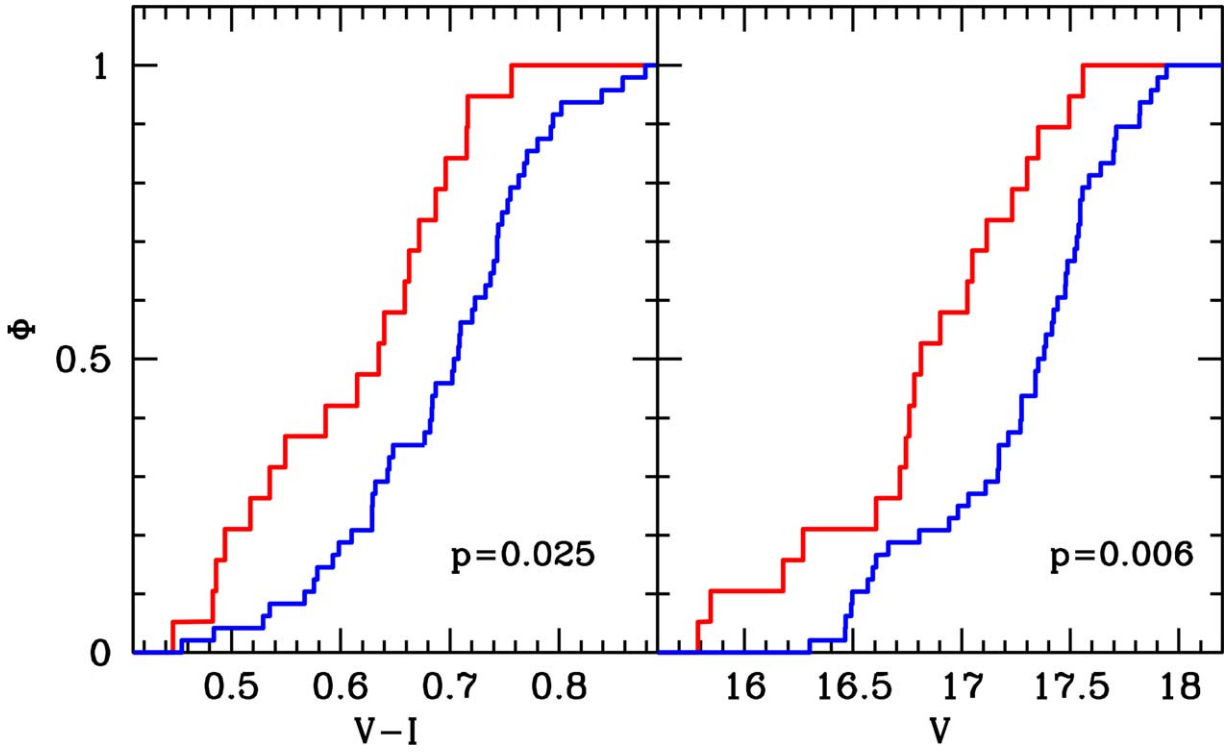


**Figure 9.** Cumulative distributions of the $(V-I)$ color (left panel) and $V$ magnitude (right panel) for the sample of FRs (i.e., BSSs with $v\sin(i) \geqslant 40$ km s$^{-1}$; red lines) and slow rotators (blue lines). The Kolmogorov–Smirnov probability to be extracted from the same parent distribution $p$ is marked in each panel. Note that the statistical significance of the Kolmogorov–Smirnov test is somehow overestimated in this case due to the need of introducing a free parameter (namely the 40 km s$^{-1}$ threshold).

dense clusters has been interpreted as the evidence of recent BSS formation from the evolution of primordial binaries, which are instead subject to the destructive action of multiple dynamical interactions in high-density environments. The case of NGC 3201 should be interpreted in this context: the measured percentage of FRs (28%) indicates an intense and recent BSS formation activity from the mass-transfer channel.

Additional information can be obtained from the analysis of the CMD and radial distributions of the observed stars. The top left panel of Figure 8 shows the CMD of NGC 3201 zoomed in the BSS region, with the slow rotators ($v\sin(i) < 40$ km s$^{-1}$) marked as small blue circles and the FRs plotted as red circles of increasing size for increasing rotational velocity. As is apparent from the figure, fast and slowly spinning BSSs are not homogeneously mixed in the CMD: FRs tend to be preferentially located in the upper left side of the BSS sequence, while the region closer to the MS-turnoff is populated by slow rotators only. This suggests the existence of a trend between the rotational velocity and the BSS luminosity and color (temperature) that is worth being further investigated.

The dependence of $v\sin(i)$ on the stellar color is shown in the upper right panel of Figure 8. Although the statistics are small, not a single FR is observed at $(V-I) > 0.75$, and a hint of decreasing rotational velocity for increasing color (i.e., decreasing surface temperature) can also be recognized. The tendency for FRs to preferentially have bluer colors than slowly spinning BSSs is also confirmed by the cumulative color distributions of the two samples that are shown in the left panel of Figure 9. The significance of the detected difference is not very high (of the order of $2.2\sigma$). However, the same signal seems to emerge (even more clearly) with the magnitude. In fact, the inspection of the bottom left panel of Figure 8 shows a tendency for the most luminous BSSs to be the faster rotators, and no slowly spinning BSSs are observed at the brightest magnitudes. Although the statistics is relatively poor, the comparison between the cumulative luminosity functions of the fast and slow rotator samples (Figure 9) seems to confirm this trend.

Thus, a general tendency to find fast-spinning BSSs at higher luminosity and at bluer colors (higher temperatures) is emerging from this study. The observed trend might also be read in terms of stellar mass (see the set of single-star evolutionary tracks overplotted as red lines in the upper left panel of Figure 8). Indeed, it is generally accepted that more luminous BSSs are more massive than their lower-luminosity sisters,[9] and such a connection between mass and luminosity is also confirmed by the observed radial distribution (see the bottom right panel of Figures 8 and 10): highly spinning BSSs (corresponding to the brighter, more massive objects) are not found in the external regions of the cluster and tend to be preferentially located toward the center. This is consistent with an effect of mass segregation. Indeed, according to the value of the $A^{+}_{\rm rh}$ parameter (Ferraro et al. 2023), NGC 3201 has an intermediate dynamical age, thus implying that dynamical friction is currently effective in making the heavier stars sink toward the cluster center starting from the most massive ones (notably, 13 out of 19 FRs, i.e., almost ∼70% of the total,

[9] Although caution must be used in deriving BSS masses from their luminosity distribution (e.g., Geller & Mathieu 2011), a reasonable agreement has been found (Raso et al. 2019) between the mass derived from fitting the spectral energy distribution and that obtained from the comparison of the BSS location in the CMD with single-star evolutionary tracks.

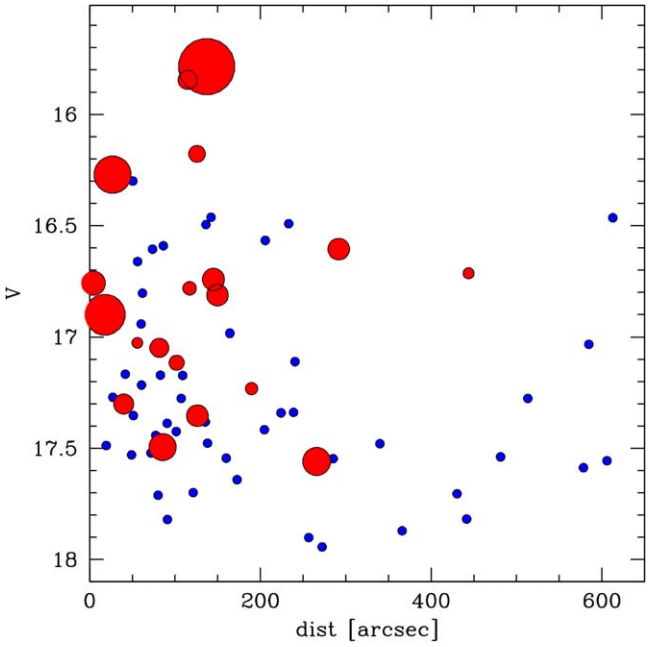


**Figure 10.** Distribution of magnitude as a function of the distance from the cluster center (in arcseconds) for the observed sample of BSSs. Symbols have the same meaning as Figure 8.

appear to be more massive than 1 $M_{\odot}$, according to the evolutionary tracks shown in the upper left panel of Figure 8).

How can the observed trend between rotational velocity and temperature (mass) be interpreted? Indeed, a decrease of rotational velocity for decreasing surface temperature has been observed also in the BSS population of the open cluster NGC 188 (Mathieu & Geller 2009). Under the hypothesis that BSS rapid rotation in low-density environments is due to mass transfer, followed by a braking timescale of the order 1–2 Gyr, the rapid rotation of more massive BSSs in NGC 3201 may indicate that the most recent BSS formation activity preferentially involved more massive primordial binaries. Alternatively, it is worth noticing that normal MS stars show a similar trend, with an increasing rotation in higher-temperature objects ($V-I<0.6$) that is attributed to their reduced convective envelopes, leading to much lengthened spin-down times (see, e.g., Kraft 1967; van Saders & Pinsonneault 2013). Hence, a similar process could be active also in the interior of BSSs, and this would be consistent with the hypothesis that most of these stars in NGC 3201 are generated from the evolution of binary systems: in fact, no convective envelope is predicted to develop in collisional products (Sills et al. 2005). Although the internal structure of BSSs is still poorly constrained, the connection of rotation with mass and temperature might be a useful clue for improved BSS models.

In conclusion, the statistical significance of the discussed trends is admittedly low, and many crucial pieces of information are still missing (including information about the binarity of these systems and their possible tidal synchronization; for recent results in the field and open clusters, see, e.g., Lurie et al. 2017; Leiner et al. 2019 and references therein). However, the results presented in this work can be considered as the starting point for future observational campaigns and possible clues for improved theoretical models aimed at properly describing the physical properties of these puzzling stars and the role that the host environment can play in setting them.

## Acknowledgments

We warmly thank the anonymous referee for the careful revision of the manuscript and the provided comments, which helped to improve the presentation of the results. This work is part of the project *Cosmic-Lab ("Globular Clusters as Cosmic Laboratories")* at the Physics and Astronomy Department "A. Righi" of the Bologna University (http://www.cosmic-lab.eu/Cosmic-Lab/Home.html). The research was funded by the MIUR throughout the PRIN-2017 grant awarded to the project *Light-on-Dark* (PI: Ferraro) through contract PRIN-2017K7REXT. A.B. acknowledges funding from the European Union NextGenerationEU.

## ORCID iDs

Alex Billi https://orcid.org/0000-0002-3810-7343
Francesco R. Ferraro https://orcid.org/0000-0002-2165-8528
Alessio Mucciarelli https://orcid.org/0000-0001-9158-8580
Barbara Lanzoni https://orcid.org/0000-0001-5613-4938
Mario Cadelano https://orcid.org/0000-0002-5038-3914
Lorenzo Monaco https://orcid.org/0000-0002-3148-9836
Mario Mateo https://orcid.org/0000-0002-3856-232X
John I. Bailey, III https://orcid.org/0000-0002-4272-263X
Megan Reiter https://orcid.org/0000-0002-3887-6185
Edward W. Olszewski https://orcid.org/0000-0002-7157-500X

## References

Alessandrini, E., Lanzoni, B., Ferraro, F. R., et al. 2016, ApJ, 833, 252
Andronov, N., Pinsonneault, M. H., & Terndrup, D. M. 2006, ApJ, 646, 1160
Beccari, G., Ferraro, F. R., Dalessandro, E., et al. 2019, ApJ, 876, 87
Benz, W., & Hills, J. G. 1987, ApJ, 323, 614
Cadelano, M., Ferraro, F. R., Dalessandro, E., et al. 2022, ApJ, 941, 69
Cadelano, M., Saracino, S., Dalessandro, E., et al. 2020, ApJ, 895, 54
Carraro, G., Vázquez, R. A., & Moitinho, A. 2008, A&A, 482, 777
Castelli, F., Gratton, R. G., & Kurucz, R. L. 1997, A&A, 318, 841
Castelli, F., & Kurucz, R. L. 2003, in IAU Symp. 210, Modelling of Stellar Atmospheres, ed. N. Piskunov et al. (Cambridge: Cambridge Univ. Press), A20
Chatterjee, S., Rasio, F. A., Sills, A., et al. 2013, ApJ, 777, 106
Clarkson, W. I., Sahu, K. C., Anderson, J., et al. 2011, ApJ, 735, 37
Cordoni, G., Milone, A. P., Marino, A. F., et al. 2023, A&A, 672, A29
Cortés, C., Silva, J. R. P., Recio-Blanco, A., et al. 2009, ApJ, 704, 750
Dalessandro, E., Ferraro, F. R., Massari, D., et al. 2013, ApJ, 778, 135
Dalessandro, E., Lanzoni, B., Ferraro, F. R., et al. 2008, ApJ, 681, 311
De Marco, O., Shara, M. M., Zurek, D., et al. 2005, ApJ, 632, 894
De Medeiros, J. R., Alves, S., Udry, S., et al. 2014, A&A, 561, A126
de Mink, S. E., Langer, N., Izzard, R. G., et al. 2013, ApJ, 764, 166
Deras, D., Cadelano, M., Ferraro, F. R., et al. 2023, ApJ, 942, 104
Dresbach, F., Massari, D., Lanzoni, B., et al. 2022, ApJ, 928, 47
Ferraro, F. R., Beccari, G., Dalessandro, E., et al. 2009, Natur, 462, 1028
Ferraro, F. R., Lanzoni, B., Dalessandro, E., et al. 2012, Natur, 492, 393
Ferraro, F. R., Lanzoni, B., Dalessandro, E., et al. 2019, NatAs, 3, 1149
Ferraro, F. R., Lanzoni, B., & Dalessandro, E. 2020, RLSFN, 31, 19
Ferraro, F. R., Lanzoni, B., Raso, S., et al. 2018a, ApJ, 860, 36
Ferraro, F. R., Lanzoni, B., Vesperini, E., et al. 2023, ApJ, 950, 145
Ferraro, F. R., Mucciarelli, A., Lanzoni, B., et al. 2018b, ApJ, 860, 50
Ferraro, F. R., Mucciarelli, A., Lanzoni, B., et al. 2023, NatCo, 14, 2584
Ferraro, F. R., Paltrinieri, B., Fusi Pecci, F., et al. 1997, A&A, 324, 915
Ferraro, F. R., Paltrinieri, B., Rood, R. T., et al. 1999, ApJ, 522, 983
Ferraro, F. R., Sabbi, E., Gratton, R., et al. 2006a, ApJL, 647, L53
Ferraro, F. R., Sills, A., Rood, R. T., et al. 2003, ApJ, 588, 464
Ferraro, F. R., Sollima, A., Rood, R. T., et al. 2006b, ApJ, 638, 433
Fiorentino, G., Lanzoni, B., Dalessandro, E., et al. 2014, ApJ, 783, 34

Gallet, F., & Bouvier, J. 2015, A&A, 577, A98
Geller, A. M., & Mathieu, R. D. 2011, Natur, 478, 356
Gilliland, R. L., Bono, G., Edmonds, P. D., et al. 1998, ApJ, 507, 818
Gosnell, N. M., Mathieu, R. D., Geller, A. M., et al. 2014, ApJL, 783, L8
Gosnell, N. M., Mathieu, R. D., Geller, A. M., et al. 2015, ApJ, 814, 163
Harris, W. E. 1996, AJ, 112, 1487
Hills, J. G., & Day, C. A. 1976, ApL, 17, 87
Hut, P. 1981, A&A, 99, 126
Jiang, D. 2022, ApJ, 940, 97
Kraft, R. P. 1967, ApJ, 150, 551
Kurucz, R., 1993 ATLAS9 Stellar Atmosphere Programs and 2 km/s grid. Kurucz CD-ROM No. 13. Cambridge, 13
Kurucz, R. L. 2005, MSAIS, 8, 14
Lanzoni, B., Dalessandro, E., Ferraro, F. R., et al. 2007, ApJ, 663, 267
Lanzoni, B., Ferraro, F. R., Alessandrini, E., et al. 2016, ApJL, 833, L29
Leigh, N., Sills, A., & Knigge, C. 2007, ApJ, 661, 210
Leiner, E., Mathieu, R. D., Gosnell, N. M., et al. 2018, ApJL, 869, L29
Leiner, E., Mathieu, R. D., Vanderburg, A., et al. 2019, ApJ, 881, 47
Leiner, E. M., & Geller, A. 2021, ApJ, 908, 229
Leonard, P. J. T., & Livio, M. 1995, ApJL, 447, L121
Lombardi, J. C., Jr., Rasio, F. A., & Shapiro, S. L. 1995, ApJL, 445, L117
Lovisi, L., Mucciarelli, A., Dalessandro, E., Ferraro, F. R., & Lanzoni, B. 2013a, ApJ, 778, 64
Lovisi, L., Mucciarelli, A., Ferraro, F. R., et al. 2010, ApJL, 719, L121
Lovisi, L., Mucciarelli, A., Lanzoni, B., et al. 2012, ApJL, 754, 91
Lovisi, L., Mucciarelli, A., Lanzoni, B., et al. 2013b, ApJ, 772, 148
Lucatello, S., & Gratton, R. G. 2003, A&A, 406, 691
Lurie, J. C., Vyhmeister, K., Hawley, S. L., et al. 2017, AJ, 154, 250
Mapelli, M., Ripamonti, E., Battaglia, G., et al. 2009, MNRAS, 396, 1771
Mateo, M., Bailey, J. I., III, Crane, J., et al. 2012, Proc. SPIE, 8446, 84464Y
Mateo, M., Harris, H. C., Nemec, J., et al. 1990, AJ, 100, 469
Mathieu, R. D., & Geller, A. M. 2009, Natur, 462, 1032
McCrea, W. H. 1964, MNRAS, 128, 335
Meibom, S., Mathieu, R. D., & Stassun, K. G. 2006, ApJ, 653, 621
Momany, Y., Held, E. V., Saviane, I., et al. 2007, A&A, 468, 973
Moretti, A., de Angeli, F., & Piotto, G. 2008, A&A, 483, 183
Mucciarelli, A., Lovisi, L., Ferraro, F. R., et al. 2014, ApJ, 797, 43
Packet, W. 1981, A&A, 102, 17
Perets, H. B., & Fabrycky, D. C. 2009, ApJ, 697, 1048
Pietrinferni, A., Hidalgo, S., Cassisi, S., et al. 2021, ApJ, 908, 102
Piotto, G., De Angeli, F., King, I. R., et al. 2004, ApJL, 604, L109
Portegies Zwart, S. 2019, A&A, 621, L10
Preston, G. W., & Sneden, C. 2000, AJ, 120, 1014
Raso, S., Pallanca, C., Ferraro, F. R., et al. 2019, ApJ, 879, 56
Reinoso, B., Leigh, N. W. C., Barrera-Retamal, C. M., et al. 2022, MNRAS, 509, 3724
Sandage, A. R. 1953, AJ, 58, 61
Sarna, M. J., & De Greve, J. P. 1996, QJRAS, 37, 11
Sbordone, L., Bonifacio, P., Castelli, F., et al. 2004, MSAIS, 5, 93
Shara, M. M., Saffer, R. A., & Livio, M. 1997, ApJ, 489, L59
Sills, A., Adams, T., & Davies, M. B. 2005, MNRAS, 358, 716
Simunovic, M., & Puzia, T. H. 2014, ApJ, 782, 49
Sollima, A., Lanzoni, B., Beccari, G., et al. 2008, A&A, 481, 701
Stetson, P. B., Pancino, E., Zocchi, A., et al. 2019, MNRAS, 485, 3042
Tonry, A. R., & Davis, M. 1979, AJ, 84, 1511
van Saders, J. L., & Pinsonneault, M. H. 2013, ApJ, 776, 67